

promoting access to White Rose research papers



Universities of Leeds, Sheffield and York
<http://eprints.whiterose.ac.uk/>

This is the published version of an article in **Geophysical Research Letters**, **34 (16)**

White Rose Research Online URL for this paper:

<http://eprints.whiterose.ac.uk/id/eprint/77230>

Published article:

Brooks, IM and Fowler, AM (2007) *New measure of entrainment zone structure*.
Geophysical Research Letters, 34 (16). L16808. 1 - 5. ISSN 0094-8276

<http://dx.doi.org/10.1029/2007GL030958>



A new measure of entrainment zone structure

I. M. Brooks¹ and A. M. Fowler^{1,2}

Received 11 June 2007; revised 26 July 2007; accepted 31 July 2007; published 22 August 2007.

[1] A wavelet covariance algorithm designed to objectively identify the upper and lower limits of the local transition zone between boundary layer and free troposphere is applied to the output fields from a series of Large Eddy Simulations of the convective atmospheric boundary layer. A new measure of entrainment zone structure is defined – the normalized difference between the standard deviations of the local transition zone limits; this is found to be a function of the convective Richardson number and a predictor of normalized entrainment rate. This provides a robust and objective means for determining the Richardson number from remote sensing observations, and the basis for determining the entrainment rate. **Citation:** Brooks, I. M., and A. M. Fowler (2007), A new measure of entrainment zone structure, *Geophys. Res. Lett.*, *34*, L16808, doi:10.1029/2007GL030958.

1. Introduction

[2] Entrainment of free tropospheric air across the temperature inversion and into the boundary layer (BL) is an important factor in controlling BL growth and structure, and the formation and distribution of BL clouds. The entrainment rate cannot be measured directly but must be inferred from other measurements [Lenschow *et al.*, 1999]. In spite of extensive study the fundamental physical processes governing entrainment and their relationship with other BL properties remain poorly understood; consequently the representation of entrainment within large-scale numerical models remains inadequate [Ayotte *et al.*, 1996; Otte and Wyngaard, 2001; Fedorovich *et al.*, 2004].

[3] Entrainment is driven by turbulence within the boundary layer, and is limited by the strength of the stably stratified temperature inversion; these joint influences can be characterized via a Richardson number. Both the rate of entrainment and the depth of the entrainment zone have been shown to scale with the inverse of the Richardson number [Deardorff *et al.*, 1980; Beyrich and Gryning, 1998; Sullivan *et al.*, 1998], but the exact forms of the relationships and the extent of their applicability under different conditions remains uncertain. Parameterization of the entrainment rate in terms of entrainment zone depth has been an attractive approach, since the latter is readily measured via remote sensing techniques such as sodar or lidar [Boers and Eloranta, 1986; Flamant *et al.*, 1997; Beyrich and Gryning, 1998; Cohn and Angevine, 2000]. A definitive approach remains elusive however. Definitions of the entrainment zone have varied substantially between

studies, as have the approaches to identifying it from the raw data, and there remains no universally accepted definition. Most commonly the entrainment zone has been defined in terms of the probability distribution of a set of spatially distributed estimates of the local boundary layer depth [Deardorff *et al.*, 1980; Wilde *et al.*, 1985; Melfi *et al.*, 1985; Flamant *et al.*, 1997]. Davis *et al.* [1997] suggested that such area-averaged approaches do not characterize the true entrainment zone but the variability of BL depth, and may include variability that does not result from entrainment, but from non-turbulent process such as gravity waves or mesoscale variations in BL structure. They suggested that a more appropriate measure would be some function of the local depth of the transition between mixed layer and free troposphere air since this reflects the recent mixing history and is driven primarily by the small scale turbulent processes responsible for entrainment. Brooks [2003] developed a multi-scale wavelet covariance algorithm to identify the upper and lower limits of this transition zone from individual lidar profiles in an objective and automated manner. Here, we apply this wavelet algorithm to the output from a large eddy simulation model to study the relationship between the local transition zone, the entrainment rate, and a convective Richardson number.

2. Large Eddy Simulations

[4] Simulations of a dry convective atmospheric boundary layer were conducted with the Boussinesq version of the UK Met Office Large Eddy Model (LEM) using its standard subgrid model [Lock and MacVean, 1999]; this has been used successfully in a number of previous studies of entrainment [Lock, 1998; Lock and MacVean, 1999]. The majority of the simulations used here were run on a $100 \times 100 \times 100$ grid with a horizontal grid spacing of 50 m. The vertical grid is stretchable, and varied smoothly between a resolution of approximately 25 m in the lower part of the initial BL, through a maximum resolution of 12 m in the region around the entrainment zone – from about 100 m below the initial inversion up to approximately twice the initial BL depth – and increasing to 110 m near the top of the domain at 3 km. A number of additional simulations were conducted with finer ($\Delta x = \Delta y = 25$ m, $\Delta z_{\min} = 7.3$ m) or coarser ($\Delta z_{\min} = 22.9$ m) resolutions to assess the sensitivity of the results to grid resolution. The simulations were initialized with potential temperature profiles of a constant 300 K within the BL, an inversion layer 50 or 100 m deep with temperature jumps of between 1 and 10 K, and a constant lapse rate of 3 K km^{-1} above the BL. A passive tracer was initially set to a constant value within the BL, decreasing linearly to zero across the inversion. The surface heat flux was specified as a constant for each simulation, and a small random perturbation added to the potential temperature field in the lowest 40 m of the domain to

¹School of Earth and Environment, University of Leeds, Leeds, UK.

²Now at Department of Meteorology, University of Reading, Reading, UK.

Table 1. Simulation Initial Conditions^a

RUN ID	Initial $\Delta\theta$, K	$\overline{w'\theta'_s}$, W m^{-2} ($\overline{w'\theta'_s}$, K m s^{-1})	Notes
A	1	50 (0.0425)	
B	1	35 (0.0298)	
C	1	10 (0.0085)	
D	2	20 (0.0170)	
E	2	40 (0.0340)	
F	2	40 (0.0340)	Initial $z_i = 300$ m
G	2	60 (0.0511)	
H	2	80 (0.0682)	
I	2	30 (0.0255)	
J	4	10 (0.0085)	
K	4	80 (0.0682)	
L	1	20 (0.0170)	$\Delta x = \Delta y = 25$ m, $\Delta z_{\min} = 7.27$ m on $200 \times 200 \times 150$ grid Initial inversion depth = 100 m
M	1	20 (0.0170)	
N	1	20 (0.0170)	
O	10	100 (0.0854)	$\Delta x = \Delta y = 25$ m, $\Delta z_{\min} = 7.27$ m on $200 \times 200 \times 150$ grid

^aModel grid is $\Delta x = \Delta y = 25$ m, $\Delta z_{\min} = 12$ m on $100 \times 100 \times 100$ grid except where noted; initial $z_i = 650$ m and inversion depth = 50 m except where noted.

initialize turbulence. Approximately two hours of simulated time were required for turbulence to become fully developed and the initial inversion to be modified by entrainment so that its structure is fully determined by the forcing conditions; after this time 3D fields of temperature and the passive tracer were saved at regular intervals of approximately 15 minutes for a period of between 3 and 6 hours. Table 1 summarizes the initial conditions and grid for all the runs included in this study. The first simulations were undertaken with a 2 K inversion strength, and the surface forcing chosen to provide a wide range of Richardson numbers. Subsequent runs were made at different inversion strengths to assess whether this exerted any influence beyond that of the Richardson number. Some additional runs were undertaken to test resolution sensitivity. There are two distinct resolution sensitivities: the fundamental ability of the model to resolve the inversion and entrainment process adequately, and the effect of discretization of the upper and lower limits of the entrainment zone identified by the wavelet algorithm due to the vertical grid spacing. With the exception of case ‘O’, which had the strongest inversion, no significant change in entrainment rate was observed with finer grid spacings, we are thus confident that resolution is adequate for the cases presented. In case ‘O’ entrainment rate was overestimated, causing a departure from the scaling behaviour discussed below, when run at the default resolution due to the inability of the coarser grid to represent the sharp inversion and a higher resolution run was utilized. As vertical resolution is coarsened, the statistics of the transition zone limits become compromised due to the limitation of the number of possible values they can take; again these effects are not found to be significant for the cases presented here.

3. Results

[5] A wavelet covariance algorithm [Brooks, 2003] was applied to the vertical profile of a passive tracer at each horizontal grid point in order to identify the lower (H_1) and

upper (H_2) limits of the transition between the mixed layer and the free troposphere (Figure 1). Determination of the wavelet covariance requires the data to be on a uniformly spaced vertical profile; thus we first interpolate from the stretched model grid to uniform intervals at the maximum grid resolution. To maintain a self-consistent set of definitions for BL properties we define all the parameters used here in terms of H_1 and H_2 . The local BL top is defined as H_1 – the top of the mixed layer – and the mean BL depth, z_i , to be the domain average of H_1 . Entrainment velocity, w_e , is the rate of change of mean BL depth with time, calculated between consecutive LEM output times. A convective Richardson number is defined [Sullivan *et al.*, 1998]:

$$Ri_* = \frac{\Delta\theta}{\theta_*}, \quad (1)$$

where $\Delta\theta$ is the mean jump in potential temperature across the inversion – defined here as the domain average of the difference between the mean temperatures in the 30 m below/above the lower/upper limits of the transition zone for each vertical profile – and θ_* is the mixed layer temperature scale,

$$\theta_* = \frac{\overline{w'\theta'_s}}{w_*} \quad (2)$$

$$w_* = \left[\frac{gz_i}{\bar{\theta}} \overline{w'\theta'_s} \right]^{1/3} \quad (3)$$

where w_* is the convective velocity scale, g is gravity, $\bar{\theta}$ is the mean temperature within the mixed layer, and $\overline{w'\theta'_s}$ is the surface heat flux. For turbulence driven by thermal convection in laboratory tank experiments Deardorff *et al.* [1980] found entrainment to follow the relation

$$\frac{w_e}{w_*} = \frac{A}{Ri} \quad (4)$$

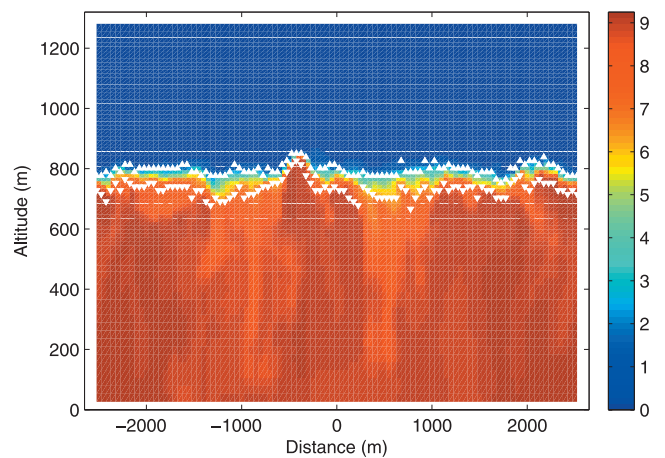


Figure 1. An example cross section of tracer concentration (arbitrary units), 4 hours into run N, with the upper (triangles) and lower (inverted triangles) limits of the transition zone indicated, as identified by the wavelet algorithm.

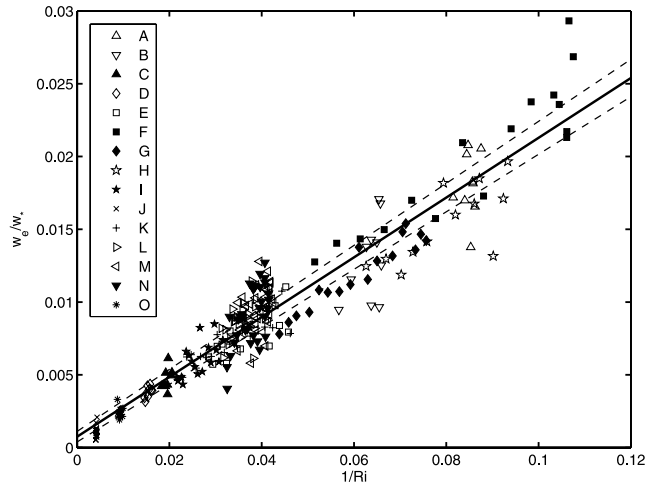


Figure 2. The normalized entrainment rate plotted against inverse Richardson number. The symbols denote individual model runs. The solid line is a best fit to the data; the dashed lines show the 95% confidence intervals to the best fit.

with A in the range $0.1 < A < 0.2$, and Ri values typical of atmospheric flows; *Sullivan et al.* [1998] found $A = 0.2$ in an LES study of a convective BL, while *Moeng and Sullivan* [1994] found A to vary with shear. Within the framework of zeroth-order jump models [*Lilly*, 1968] in which much of the study of convective entrainment has taken place, it can be shown that A is also equal to the ratio of the negative of the minimum buoyancy flux at the inversion to the surface buoyancy flux (also commonly denoted by A); this equivalence does not hold for LES results due to the finite depth of the inversion layer [*vanZanten et al.*, 1999], though the distinction is not always made. Inconsistency in the way in which A is determined between studies is partially responsible for the substantial variability in the values reported; real differences also arise due to the influence of shear [*Pino et al.*, 2003; *Conzemius and Fedorovich*, 2006; *Angevine*, 2007].

[6] Figure 2 shows the normalized entrainment rate plotted against the inverse Richardson number for all the simulations listed in Table 1. There is considerable scatter in individual values of entrainment rate, but a strong linear relationship. The line of best fit and 95% confidence intervals are shown. The gradient A is 0.21 ± 0.01 with an intercept of 0.0007 ± 0.0004 , and a correlation coefficient of 0.92; if the fit is constrained to pass through the origin then $A = 0.22 \pm 0.004$. It is noted that w^* appears in the denominator on both sides of (4); these effectively cancel, and do not introduce any spurious correlation in Figure 2; w^* is retained to maintain consistency and aid comparison with other studies.

[7] Having obtained estimates of the local transition zone limits, we need to define some non-dimensional measure of entrainment zone properties from them. A simple measure of entrainment zone depth might be the normalized average transition zone depth; however, while this might be expected to increase with turbulence intensity, we would still expect a non-zero value in the absence of active entrainment provided an inversion of finite depth existed. In order to distinguish entraining conditions from non-

entraining we consider the variability of the transition zone limits. Figure 3 shows the difference between the standard deviations of H_1 and H_2 scaled by mean BL depth and plotted against inverse Richardson number; a least-squares quadratic fit to the data is also shown. The correlation with inverse Richardson number is excellent, with a correlation coefficient of 0.97, and the fitted curve approaches zero with Ri^{-1} . Similar relationships between an entrainment zone parameter and a variety of Richardson numbers have been examined in the past; direct comparisons are difficult due to the wide variations in definitions of the key terms, but broadly similar behaviour is observed. *Sullivan et al.* [1998] plotted σ_{z1}/z_i against the same Ri used here; they did not provide a fit to the data, but obtained a roughly inverse proportionality. Numerically, their results are very close to those presented here. *Gryning and Batchvarova* [1994] examined the normalized entrainment zone depth $\Delta h/h$ (where Δh is essentially the mean inversion depth, and h the height of the mid-point of the inversion) as a function of both a convective Richardson number and an entrainment zone Richardson number in which w^* is replaced by w_e . The functional relationships obtained are similar to those found here, though $\Delta h/h$ has values about an order of magnitude larger than either our or *Sullivan et al.*'s entrainment zone parameters; they also found use of the entrainment zone Richardson number resulted in less scatter in the results.

[8] Figure 4 combines the results of Figures 2 and 3, showing normalized entrainment rate as a function of $(\sigma_{H1} - \sigma_{H2})/z_i$. The data is fitted with a power law $y = ax^b$, where $a = 0.13$, $b = 0.7$, and the correlation coefficient is 0.91. Within a given simulation, Ri^{-1} and w_e tend to increase with time, due to warming of the BL and a consequent reduction in $\Delta\theta$; thus consecutive points in time on Figures 2–4 tend to move towards the upper right. No significant difference in the scaling behaviour is observed between cases with weak and strong inversions. Small subsets of the

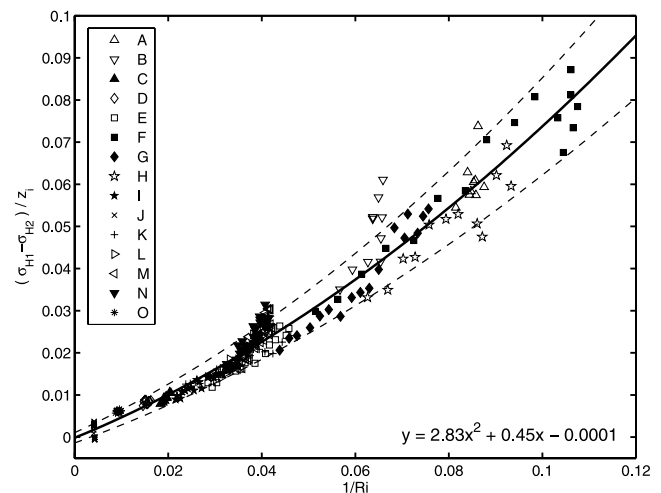


Figure 3. The difference in standard deviations of lower and upper transition zone limits normalized by mean mixed-layer depth plotted against inverse Richardson number. The solid line is a quadratic best fit to the data; the dashed lines show the 95% confidence intervals to the best fit.

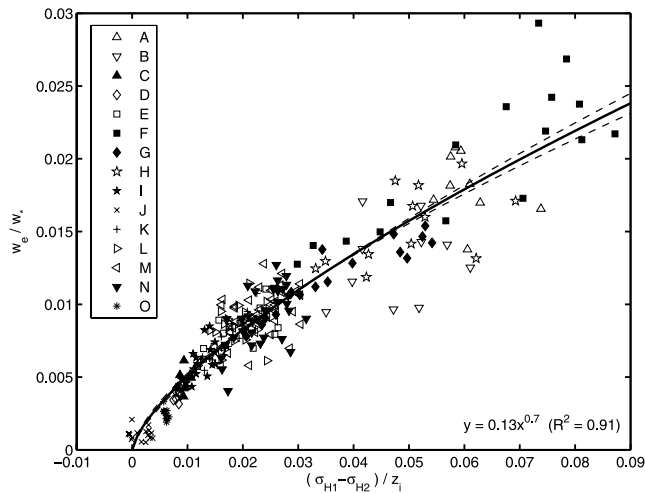


Figure 4. Normalised entrainment velocity as a function of $(\sigma_{H1} - \sigma_{H2})/z_i$. A power law is fitted (solid line) and the 95% confidence limits shown (dashed lines).

data lie closely grouped slightly above the majority of the data—though the behavior is not entirely consistent between the figures. *Sullivan et al.* [1998] identify a similar handful of points in their results, at $Ri^{-1} > 0.7$, that they suggest might indicate a regime in which a different power law applies. Further investigation is required to identify whether these cases genuinely represent a different scaling regime, and if so what change in physical processes controls the change. We note that these data all arise where the inversion is very weak (< 0.5 K), it is thus possible that they result from a change in the entrainment regime from one where the eddy scales responsible for entrainment are governed by properties of the BL as a whole rather than those of the interfacial layer. Although these points make a strong visual impression, the fitted curves are not significantly modified if they are omitted.

4. Summary and Conclusions

[9] Large eddy simulations of dry convection in the atmospheric boundary layer have been used to study some of the properties of entrainment across an inversion capping the convective boundary layer. A wavelet covariance algorithm was applied to profiles of a passive tracer to identify the upper and lower limits of the transition zone between well mixed BL and free troposphere. The entrainment rate, normalized by the convective scaling velocity, was found to be proportional to the inverse of a convective Richardson number. The constant of proportionality, A , was found to be 0.21 ± 0.01 , in close agreement with previous estimates for purely convective conditions. The entrainment zone was characterized by the difference in standard deviations of the transition zone limits, normalized by the mean mixed-layer depth; this is also found to be a function of the inverse Richardson number, approaching zero as Ri^{-1} approaches zero. The normalized entrainment rate can be related directly to $(\sigma_{H1} - \sigma_{H2})/z_i$. This result can be interpreted physically as follows: entrainment proceeds by a series of discrete mixing events that mix free troposphere air down across the

top of the inversion layer, perturbing the local value of H_2 . Once within the turbulent boundary layer, mixing proceeds more rapidly, and the entrained air is diluted and mixed over an increasing volume, perturbing the local value of H_1 . The perturbation of H_1 is both larger and longer lived than that of H_2 – this is readily seen in both lidar imagery [Brooks, 2003] and LES output fields (Figure 1). As entrainment increases, so does the difference in variability between H_1 and H_2 . If entrainment ceases, residual turbulence within the BL will sharpen the inversion, making it increasingly difficult to perturb H_1 . Our definition of entrainment velocity is the rate of change of mean value of H_1 , thus even when material has ceased to be mixed across the upper limit of the inversion, entrainment can be said to continue, increasingly weakly, while the mean value of H_1 increases as the inversion is sharpened. We note that this measure of entrainment zone structure remains an area averaged property, and is not immune to the problems noted by *Davis et al.* [1997]. The use of information about both upper and lower limits of the transition zone between the mixed layer and free troposphere, however, seems to us to provide a stronger link between this measure of entrainment zone structure and the physical processes involved than is the case for measures based on estimates of a simple BL depth because it encompasses both the initial mixing across the top of the inversion and subsequent mixing between the lower part of the inversion and mixed layer.

[10] The results presented demonstrate an objective means of utilizing remote-sensing data to estimate the convective Richardson number and the relative strength of entrainment directly, without any other information on the BL properties. The addition of a potential temperature profile, for example from a radiosonde, would allow the mean mixed layer temperature and jump across the inversion to be determined, and provides sufficient information to make estimates of the surface heat flux, w^* , θ^* , and the true entrainment velocity. This might provide a means for estimating bulk turbulence properties and entrainment rate operationally or over remote locations, such as the oceans, from routine observations such as laser ceilometers or satellite borne lidars coupled with radiosonde profiles or mean profiles from large-scale forecast models.

[11] **Acknowledgments.** AMF was supported by an M.Res. studentship from the Natural Environment Research Council while undertaking this study. We would like to thank Wayne Angevine, Ken Davis, and Jeff Grabon for their constructive comments on earlier versions of the manuscript.

References

- Angevine, W. M. (2007), Transitional, entraining, cloudy, and coastal boundary layers, *Acta Geophys.*, in press.
- Ayotte, K. W., et al. (1996), An evaluation of neutral and convective planetary boundary layer parameterizations relative to large eddy simulations, *Boundary Layer Meteorol.*, *79*, 131–175.
- Beyrich, F., and S.-E. Gryning (1998), Estimation of the entrainment zone depth in a shallow convective boundary layer from sodar data, *J. Appl. Meteorol.*, *37*, 255–268.
- Boers, R., and E. W. Eloranta (1986), Lidar measurements of the atmospheric entrainment zone and the potential temperature jump across the top of the mixed layer, *Boundary Layer Meteorol.*, *34*, 357–375.
- Brooks, I. M. (2003), Finding boundary layer top: Application of a wavelet covariance transform to lidar backscatter profiles, *J. Atmos. Oceanic Technol.*, *20*, 1092–1105.
- Cohn, S. A., and W. M. Angevine (2000), Boundary-layer height and entrainment zone thickness measured by lidars and wind profiling radars, *J. Appl. Meteorol.*, *39*, 1233–1247.

- Conzemius, R. J., and E. Fedorovich (2006), Dynamics of sheared convective boundary layer entrainment. Part I: Methodological background and large-eddy simulations, *J. Atmos. Sci.*, *63*, 1151–1912.
- Davis, K. J., D. H. Lenschow, S. P. Oncley, C. Kiemle, G. Ehret, A. Giez, and J. Mann (1997), Role of entrainment in surface-atmosphere interactions over the boreal forest, *J. Geophys. Res.*, *102*, 29,219–29,230.
- Deardorff, J. W., G. E. Willis, and B. H. Stockton (1980), Laboratory studies of the entrainment zone of a convectively mixed layer, *J. Fluid Mech.*, *100*, 41–64.
- Fedorovich, E., R. Conzemius, and D. Mironov (2004), Convective entrainment into a shear-free, linearly stratified atmosphere: Bulk models re-evaluated through large eddy simulations, *J. Atmos. Sci.*, *61*, 281–295.
- Flamant, C., J. Pelon, P. H. Flamant, and P. Durand (1997), Lidar determination of the entrainment zone thickness at the top of the unstable marine atmospheric boundary layer, *Boundary Layer Meteorol.*, *83*, 247–284.
- Gryning, S.-E., and E. Batchvarova (1994), Parameterization of the depth of the entrainment zone above the daytime mixed layer, *Q. J. R. Meteorol. Soc.*, *120*, 47–58.
- Lenschow, D. H., P. B. Krummel, and S. T. Siems (1999), Measuring entrainment, divergence, and vorticity on the mesoscale from aircraft, *J. Atmos. Oceanic Technol.*, *16*, 1384–1400.
- Lilly, D. K. (1968), Models of cloud-topped mixed layers under a strong inversion, *Q. J. R. Meteorol. Soc.*, *94*, 292–309.
- Lock, A. P. (1998), The parameterization of entrainment in cloudy boundary layers, *Q. J. R. Meteorol. Soc.*, *124*, 2729–2753.
- Lock, A. P., and M. K. MacVean (1999), The generation of turbulence and entrainment by buoyancy reversal, *Q. J. R. Meteorol. Soc.*, *125*, 1017–1038.
- Melfi, S. H., J. D. Sphinime, S. H. Chou, and S. P. Palm (1985), Lidar observations of the vertically organized convection in the planetary boundary layer over the ocean, *J. Clim. Appl. Meteorol.*, *24*, 806–821.
- Moeng, C. H., and P. P. Sullivan (1994), A comparison of shear and buoyancy driven planetary-boundary-layer flows, *J. Atmos. Sci.*, *51*, 999–1022.
- Otte, M. J., and J. C. Wyngaard (2001), Stably stratified interfacial-layer turbulence from large eddy simulations, *J. Atmos. Sci.*, *58*, 3424–3442.
- Pino, D., J. Vila-Guerau de Arellano, and P. G. Duynkerke (2003), The contribution of shear to the evolution of a convective boundary layer, *J. Atmos. Sci.*, *60*, 1913–1926.
- Sullivan, P. P., C.-H. Moeng, B. Stevens, D. H. Lenschow, and S. H. Mayor (1998), Structure of the entrainment zone capping the convective atmospheric boundary layer, *J. Atmos. Sci.*, *55*, 3042–3064.
- vanZanten, M. C., P. G. Duynkerke, and J. W. M. Cuijpers (1999), Entrainment parameterization in convective boundary layers, *J. Atmos. Sci.*, *56*, 813–828.
- Wilde, N. P., R. B. Stull, and E. W. Eloranta (1985), The LCL zone and cumulus onset, *J. Clim. Appl. Meteorol.*, *24*, 640–657.

I. M. Brooks, School of Earth and Environment, University of Leeds, Leeds LS2 9JT, UK. (i.brooks@see.leeds.ac.uk)

A. M. Fowler, Department of Meteorology, University of Reading, Earley Gate, P.O. Box 243, Reading RG6 6BB, UK. (a.m.fowler@reading.ac.uk)